ISSN 1063-7737, Astronomy Letters, 2013, Vol. 39, No. 1, pp. 54–64. © Pleiades Publishing, Inc., 2013.
Original Russian Text © Yu.V. Pakhomov, 2013, published in Pis'ma v Astronomicheskiĭ Zhurnal, 2013, Vol. 39, No. 1, pp. 58–69.

Sodium in the Atmospheres of Thick-Disk Red Giants

Yu. V. Pakhomov*

Institute of Astronomy, Russian Academy of Sciences, Pyatnitskaya ul. 48, Moscow, 109017 Russia

Received August 28, 2012

Abstract—The atmospheric parameters and elemental abundances for ten thick-disk red giants have been determined from high-resolution spectra by the method of model stellar atmospheres. The results of a comparative analysis of the [Na/Fe] abundances in the atmospheres of the investigated stars and thin-disk red giants are presented. Sodium in the atmospheres of thick-disk red giants is shown to have no overabundances typical of thin-disk red giants.

DOI: 10.1134/S1063773713010015

Keywords: *stellar spectroscopy, stellar atmospheres, red giants, stellar evolution, kinematics, Galactic chemical evolution.*

INTRODUCTION

The abundances of chemical elements in the atmospheres of stars are known to change in the course of their evolution. When investigating the chemical composition of giants, the first to be detected were the CNO abundance anomalies compared to the chemical composition of dwarf stars (see, e.g., Schopp 1954; Greenstein and Keenan 1958; Helfer et al. 1959; Greene 1968). The observed sodium overabundance in the atmosphere of the red giant ϵ *Vir* was first mentioned in 1963 (G. Cayrel and R. Cayrel 1963). Subsequently, sodium overabundances were detected in red giants of the Hyades open cluster (Helfer and Wallerstein 1964). In another paper (Helfer and Wallerstein 1968), the same authors found several giants with a [Na/Fe] overabundance and may have been the first to point out a systematic difference in sodium abundance between red giants and dwarfs. They hypothesized that sodium might be synthesized in some red giants. Slightly later, in 1970 (Cayrel de Strobel et al. 1970) noted that the [Na/Fe] abundance increases with temperature parameter $\theta = 5040/T_{\rm eff}$. In other words, the [Na/Fe] abundance in cooler stars turned out to be, on average, higher, while giants are in the majority among these stars, i.e., the sodium abundance difference between dwarfs and giants is also noticeable, although the authors did not reach this conclusion.

Boyarchuk et al. (2001) were the first to describe the dependence of the [Na/Fe] overabundances in the atmospheres of normal red giants on surface gravity. This dependence turned out to be similar to that discovered previously for supergiants (A. Boyarchuk and M. Boyarchuk 1981; Boyarchuk and Lyubimkov 1981). It was explained by the hypothesis that sodium could be produced in the $^{22}{\rm Ne}(p,\gamma)^{23}{\rm Na}$ reaction entering the neon–sodium cycle of hydrogen burning in the cores of main-sequence stars and could then be brought from deep layers into the stellar atmosphere through developing convection as the star evolves from the main sequence to the red giant branch (Boyarchuk and Lyubimkov 1983). The calculations performed by Denisenkov and Ivanov (1987) and Denisenkov (1988) confirmed the validity of this hypothesis. Further studies revealed [Na/Fe] overabundances in the atmospheres of various classes of red giants: moderate and classical barium stars (Boyarchuk et al. 2002; Antipova et al. 2004), super-metal-rich stars (Pakhomov et al. 2009). A database of characteristics for red giants was created from the accumulated material at the Institute of Astronomy, the Russian Academy of Sciences. Our studies using the database revealed several stars with a [Na/Fe] underabundance relative to the observed dependence on surface gravity (Antipova et al. 2005; Pakhomov et al. 2009). A comparative analysis showed that these stars are distinguished by slightly higher space velocities. To confirm this conclusion, we investigated the chemical composition of red giants with high Galactic velocities (Pakhomov et al. 2012) and pointed out that 12 of the 14 investigated stars also have a [Na/Fe] underabundance.

*E-mail: pakhomov@inasan.ru

There exist quite a few works devoted to the abundance analysis of Galactic thin- and thick-disk stars. These works are based on spectroscopic observations of dwarfs, because their atmospheric elemental abundances undergo no changes as they evolve on the main sequence. Besides, in comparison with giants, dwarfs form a larger group and their continuum spectrum exhibits a smaller number of spectral lines, which increases the accuracy of abundance determinations. Therefore, there are comparatively few works devoted to thick-disk giants. There are even fewer studies of sodium in thick-disk giants (see, e.g., Smiljanic 2012; Alves-Brito et al. 2010). In these papers, the dependences of the [Na/Fe] abundance on mass and metallicity are discussed, but such an important factor as the evolutionary status is overlooked. Since the sodium abundances in stellar atmospheres do not appear instantaneously but gradually increase since the first deep mixing, the evolutionary stage of the star should be taken into account.

In this paper, we perform a comparative analysis of the [Na/Fe] abundance in the atmospheres of thin- and thick-disk red giants as a function of their metallicity and surface gravity, which changes during the lifetime of a star. Thus, investigating the changes in the atmospheric sodium abundance of red giants is necessary for understanding the stellar evolution, while the detected sodium underabundance in thick-disk giants requires a further study.

OBSERVATIONS

Selection of Stars

We selected the objects for our observations from the Hipparcos catalogue (van Leeuwen 2007) by analyzing the Galactic velocities (UVW) calculated using reduced Hipparcos parallaxes and CORAVEL radial velocities (Maurice et al. 1987). The selection criteria were the ($B-V$) color indices and calculated surface gravities corresponding to red giants; the calculated Galactic velocities exceeding those typical of thin-disk stars (34.5, 22.5, 18.0) km s^{-1} (Famaey et al. 2005), with $W > 50$ km s^{-1}.

The list of program stars is presented in Table 1, where their ordinal numbers, HD numbers, coordinates, V magnitudes, and spectral types are given. The last two columns in Table 1 provide the membership probabilities of the program stars in the Galactic thin and thick disks, whose kinematic characteristics were taken from Famaey et al. (2005). The probabilities were calculated using formulas from Mishenina et al. (2004). It can be seen from the table that all stars can be assigned to thick-disk objects with a high probability.

Table 2 presents kinematic characteristics of the investigated stars. These include the Galactic velocity vector (U, V, W) relative to the Sun and Galactic orbital elements: the perigalactic distance $R_{\min}$, the apogalactic distance $R_{\max}$, the maximum orbital distance from the Galactic plane $Z_{\max}$, the eccentricity e, and the inclination i. The distance to the Galactic center was assumed to be 8.5 kpc, while the necessary correction of the velocities for the solar motion, (+10.2, +14.9, +7.8) km s^{-1}, was taken from Famaey et al. (2005). We calculated the orbital elements through numerical integration of the stellar motion by Everhart's 15th-order method using a three-component model Galactic potential (Allen and Santillan 1991). The integration accuracy was controlled by the conservation of the necessary integrals of motion. For example, in ten orbital revolutions, the typical relative error was $\Delta h/h < 10^{-13}$ in angular momentum and $\Delta E/E < 10^{-8}$ in total energy. The errors in the space velocities ($\sigma U, \sigma V, \sigma W$) were calculated from the errors in the stellar proper motions, radial velocities, parallaxes and the errors in the solar velocity components relative to the local standard of rest. We calculated the errors in the Galactic orbital elements based on the model Galactic gravitational potential using the probable errors in the stellar space velocities.

It can be seen from Table 2 that all stars have a maximum orbital distance from the Galactic plane $Z_{\max} > 1000$ pc, which exceeds considerably the characteristic scale height for thin-disk objects, 90–325 pc (Gilmore and Reid 1983; Robin et al. 1996; Chen et al. 2001). More than half of the investigated stars have orbits with eccentricities larger than 0.2. About half of the stars recede to a distance of more than 10 kpc from the Galactic center when moving in their orbits.

Spectroscopic Observations and Their Reduction

The spectroscopic observations of the selected stars were performed in 2010 with a two-band echelle spectrograph attached to a 2.16-m telescope at the Xinglong station of the National Astronomical Observatories of China (NAOC). The spectrograph operated in the red-band mode. The detector was a 2048 × 2048 CCD array on which 45 spectral orders in the range from 5500 to 9830 Å were recorded. The spectrograph resolution was $R = 40\,000$; the signal-to-noise ratio in the spectra was $S/N > 100$.

The *echelle* package of the *MIDAS* software system was used for the preliminary spectroscopic data reduction, the search for and extraction of the spectral orders, the wavelength calibration using the spectrum of a thorium–argon lamp, and the spectrum normalization.

Table 1. The list of investigated stars with the membership probabilities (p) in the Galactic thin and thick disks

N	HD	α_{2000} h:m:s	δ_{2000} ° : ′ : ″	m_V	Spectral type	p, %	
						thin disk	thick disk
1	249	00 07 22.56332	+26 27 02.1686	7.33	K1IV	0	99
2	6555	01 06 38.62642	+23 13 57.4834	7.95	K0III-IV	15	84
3	10057	01 38 19.91771	+02 35 09.8395	6.92	K0	1	97
4	24758	03 59 17.62739	+57 59 13.6255	8.67	K0III	0	99
5	37171	05 37 04.38211	+11 02 06.0293	6.00	K5III	0	99
6	80966	09 23 50.43122	+34 32 53.3986	7.17	K0	0	99
7	180682	19 15 43.69429	+40 21 35.7242	6.96	K0	0	99
8	203344	21 21 04.39426	+23 51 21.4872	5.57	K1III	0	99
9	211683	22 18 37.60252	+10 21 18.7937	7.73	K2	20	79
10	212074	22 21 27.94691	+14 53 49.6214	7.64	K1IV	3	96

Table 2. Kinematic parameters of the investigated stars: the Galactic velocity vector components (U, V, W) and Galactic orbital elements

N	HD	U, km s^{-1}	V, km s^{-1}	W, km s^{-1}	$R_{\min}$, kpc	$R_{\max}$, kpc	$Z_{\max}$, kpc	e
1	249	45.4 ± 3.1	-55.5 ± 5.2	-78.6 ± 5.3	6.00 ± 0.14	8.93 ± 0.04	1.46 ± 0.09	0.20 ± 0.01
2	6555	-25.0 ± 4.0	-12.1 ± 3.0	-68.3 ± 5.8	7.98 ± 0.06	10.04 ± 0.13	1.21 ± 0.10	0.11 ± 0.01
3	10057	3.6 ± 7.1	-46.8 ± 7.0	55.6 ± 1.3	6.90 ± 0.24	8.70 ± 0.02	1.38 ± 0.02	0.12 ± 0.02
4	24758	-123.7 ± 4.3	-23.8 ± 7.9	-84.2 ± 13.8	5.98 ± 0.12	14.64 ± 0.38	2.36 ± 0.41	0.42 ± 0.01
5	37171	-113.1 ± 0.8	-19.0 ± 10.4	65.2 ± 9.5	6.15 ± 0.15	14.42 ± 0.42	2.18 ± 0.25	0.40 ± 0.00
6	80966	-23.4 ± 14.0	-105.4 ± 23.8	75.5 ± 9.5	3.92 ± 0.56	8.83 ± 0.08	2.15 ± 0.19	0.39 ± 0.06
7	180682	-89.7 ± 8.7	-11.6 ± 4.2	59.6 ± 5.7	6.72 ± 0.10	12.70 ± 0.31	1.70 ± 0.13	0.31 ± 0.02
8	203344	61.5 ± 1.0	-102.4 ± 0.6	-70.1 ± 2.5	3.69 ± 0.02	8.86 ± 0.01	1.21 ± 0.05	0.41 ± 0.00
9	211683	-7.1 ± 4.4	-20.2 ± 3.3	50.2 ± 5.7	8.12 ± 0.09	8.75 ± 0.11	1.06 ± 0.08	0.04 ± 0.01
10	212074	-6.2 ± 3.0	-5.9 ± 5.5	61.5 ± 8.7	8.34 ± 0.02	9.94 ± 0.27	1.46 ± 0.16	0.09 ± 0.01

The equivalent widths of the selected spectral lines were measured in the *EW* code that I developed. The code is a set of modules written in Perl and C, the access to which is organized via a graphical user interface. The automatic equivalent width determination module is the main one in the code. It uses the nonlinear Levenberg–Marquardt algorithm from the *PDL* package. For each measured spectral line with wavelength λ_0, the part of the spectrum $\lambda_0 \pm 10\lambda_0/R$ in which the spectral lines are searched for is cut out. An iterative deconvolution method is applied for a better line detection; it allows the blends to be separated. More or less significant lines can be identified by varying the number of iterations. Each spectral line is fitted by a Gaussian, which is a normal approximation for most of the lines with equivalent widths <100 mÅ. The investigated part of the spectrum is fitted by the sum of Gaussians $F(\lambda) = \sum_{i=0}^{k} h_i * e^{-(\lambda_i - \lambda_0)^2/\sigma_i^2}$, where h_i and σ_i are the depth and width of the ith spectral line. We take the depth

Table 3. Atmospheric parameters of the investigated stars, their masses, and interstellar extinctions

N	HD	$T_{\rm eff}$, K	$\log g$	V_t, km s^{-1}	[Fe/H]	Mass, $M_\odot$	A_V, m
1	249	4850	2.96	1.17	−0.15	1.5 ± 0.2	0
2	6555	4720	3.00	1.15	−0.09	1.2 ± 0.2	<0.1
3	10057	4130	1.70	1.35	−0.30	1.7 ± 0.3	0.3
4	24758	4680	2.75	1.15	0.11	1.4 ± 0.2	0
5	37171	4000	1.25	1.35	−0.55	1.1 ± 0.2	0.5
6	80966	4550	1.80	1.50	−1.01	1.2 ± 0.3	<0.1
7	180682	4330	1.90	1.40	−0.43	1.1 ± 0.2	0.3
8	203344	4770	2.75	1.30	−0.09	1.8 ± 0.2	0
9	211683	4450	1.80	1.35	−0.13	1.9 ± 0.3	0.3
10	212074	4700	2.55	1.30	0.05	2.3 ± 0.3	<0.1

of the observed line as the initial approximation for h and $\sigma = \lambda_0/R$ for the width. The module operation result is a set of parameters of the Gaussians that best fit the observed spectrum. The parameters of the investigated spectral line are written in a file. In addition, information about the quality of the fit and the degree of line blending is written. During its operation, the code displays a theoretical spectrum of atomic and molecular lines that provides an additional possibility for the selection of lines.

DETERMINATION OF STELLAR ATMOSPHERE PARAMETERS

We determined the stellar atmosphere parameters using a technique based on Kurucz's model atmospheres (Castelli and Kurucz 2003) and analysis of the relative abundances of iron-peak elements. The technique is described in detail in Boyarchuk et al. (2001) and allows the stellar atmosphere parameters for G–K giants to be determined with an accuracy of about 70–100 K for $T_{\rm eff}$, 0.10–0.15 for $\log g$, and 0.10–0.15 km s^{-1} for V_t. For late-K giants, the accuracy can be lower due to the greater influence of blending by atomic and molecular lines. In this paper, when analyzing the relative abundances of iron-peak elements when determining the stellar atmosphere parameters, we disregarded titanium, because it is well known that the [Ti/Fe] abundance can be enhanced at low metallicities and for thick-disk stars (Bensby et al. 2005). Using the derived parameters ($T_{\rm eff}$, $\log g$, V_t), we computed the corresponding model stellar atmospheres with the ATLAS9 code (Kurucz 1993).

Table 3 gives our estimates of the stellar atmosphere parameters (effective temperature $T_{\rm eff}$, surface gravity $\log g$, microturbulence V_t, and metallicity [Fe/H]), masses, and interstellar extinctions A_V. We determined the masses based on evolutionary tracks from Girardi et al. (2000) by taking into account the stellar metallicity. The interstellar extinctions were estimated from the color excess $E(B-V)$; the dereddened colors were calculated from calibrations (Bessell et al. 1998) based on Kurucz's model stellar atmospheres.

Based on the measured equivalent widths of the selected unblended spectral lines, we estimated the elemental abundances with the WIDTH9 code. These are presented in Table 4 and Fig. 1, where the open circles and asterisks denote the abundances determined from the spectral lines of neutral and ionized atoms, respectively. The list of selected lines with their characteristics and equivalent widths is available in electronic form. The cobalt abundance was determined by taking into account the hyperfine splitting effect, which can be strong in the case of cool giants (Boyarchuk et al. 2008). The abundance errors given in Table 4 and marked by the bars in Fig. 1 were determined as the dispersion of the individual abundances calculated from individual spectral lines. As an example, the possible abundance errors associated with the determination of stellar atmosphere parameters are listed in Table 5 for two stars. Table 5 gives the number of lines used (N) and the changes in the abundance of each element when changing individual model parameters ($\Delta T_{\rm eff} = +100$ K, $\Delta \log g = +0.10$, $\Delta V_t = +0.10$ km s^{-1}) and the total change in abundance Δ.

Table 4. Elemental abundances in the atmospheres of the investigated stars

Element	HD 249		HD 6555		HD 10057		HD 24758		HD 37171	
	N	[X/H]	N	[X/H]	N	[X/H]	N	[X/H]	*N*	[X/H]
Na I	2	-0.23 ± 0.04	2	-0.03 ± 0.09	2	-0.26 ± 0.08	2	0.33 ± 0.07	1	-0.66
Mg I	2	-0.03 ± 0.02	2	0.17 ± 0.04	2	-0.06 ± 0.04	2	0.21 ± 0.03	2	-0.29 ± 0.08
Al I	2	0.06 ± 0.02	2	0.20 ± 0.01	2	0.05 ± 0.09	2	0.20 ± 0.01	2	-0.19 ± 0.05
Si I	9	-0.15 ± 0.05	9	0.02 ± 0.07	4	-0.23 ± 0.07	12	0.18 ± 0.08	5	-0.48 ± 0.07
Ca I	4	0.03 ± 0.04	3	0.02 ± 0.02	3	-0.13 ± 0.06	3	0.11 ± 0.04	2	-0.35 ± 0.02
Sc I	2	-0.01 ± 0.10	2	0.14 ± 0.08	1	-0.05	2	0.17 ± 0.04	–	–
Sc II	3	0.02 ± 0.09	5	0.11 ± 0.06	6	-0.14 ± 0.05	5	0.11 ± 0.06	5	-0.34 ± 0.07
Ti I	21	-0.06 ± 0.08	32	0.04 ± 0.08	18	-0.23 ± 0.07	26	0.00 ± 0.05	16	-0.32 ± 0.05
V I	18	-0.02 ± 0.05	24	0.09 ± 0.09	2	-0.24 ± 0.01	19	0.14 ± 0.07	3	-0.31 ± 0.09
Cr I	6	-0.24 ± 0.07	6	-0.12 ± 0.05	8	-0.38 ± 0.06	12	0.12 ± 0.07	7	-0.70 ± 0.08
Mn I	1	-0.25	1	-0.30	1	-0.69	1	-0.07	1	-0.91
Fe I	71	-0.15 ± 0.07	88	-0.09 ± 0.07	64	-0.30 ± 0.07	80	0.11 ± 0.06	34	-0.55 ± 0.08
Fe II	5	-0.24 ± 0.07	6	-0.14 ± 0.07	4	-0.39 ± 0.02	7	0.09 ± 0.05	2	-0.68 ± 0.06
Co I	5	-0.19 ± 0.09	6	-0.07 ± 0.10	3	-0.33 ± 0.02	6	-0.02 ± 0.14	4	-0.55 ± 0.04
Ni I	21	-0.15 ± 0.08	26	-0.04 ± 0.06	20	-0.35 ± 0.07	22	0.20 ± 0.06	5	-0.60 ± 0.04
Y II	–	–	–	–	–	–	1	-0.08	2	-0.77 ± 0.11
Zr II	–	–	–	–	1	-0.49	–	–	1	-0.41
Ba II	–	–	1	0.06	1	-0.22	1	0.03	1	-0.02
La II	1	0.34	–	–	1	-0.32	–	–	–	–
Nd II	1	0.02	1	0.01	1	-0.10	1	-0.13	2	-0.32 ± 0.12
Eu II	–	–	1	0.10	–	–	1	-0.04	1	-0.15

Element	HD 80966		HD 180682		HD 203344		HD 211683		HD 212074	
	N	[X/H]	N	[X/H]	N	[X/H]	N	[X/H]	N	[X/H]
Na I	2	-1.22 ± 0.02	2	-0.36 ± 0.04	2	-0.03 ± 0.11	2	-0.07 ± 0.15	2	0.04 ± 0.07
Mg I	2	-0.60 ± 0.06	2	-0.12 ± 0.04	2	0.16 ± 0.01	2	0.08 ± 0.05	2	0.26 ± 0.05
Al I	2	-0.72 ± 0.02	2	-0.10 ± 0.04	2	0.18 ± 0.05	2	0.15 ± 0.04	2	0.20 ± 0.05
SivI	9	-0.65 ± 0.03	7	-0.25 ± 0.04	9	0.06 ± 0.06	8	-0.12 ± 0.09	11	0.08 ± 0.08
Ca I	6	-0.72 ± 0.04	3	-0.19 ± 0.04	4	0.10 ± 0.07	2	0.11 ± 0.08	3	0.18 ± 0.08
Sc I	1	-1.73	1	-0.18	2	0.10 ± 0.08	–	–	2	0.15 ± 0.07
Sc II	6	-0.96 ± 0.05	7	-0.20 ± 0.04	4	0.18 ± 0.04	3	-0.04 ± 0.07	7	0.15 ± 0.06
Ti I	22	-0.79 ± 0.05	22	-0.23 ± 0.07	21	0.05 ± 0.06	14	0.01 ± 0.04	25	0.06 ± 0.06
V I	16	-0.99 ± 0.06	7	-0.16 ± 0.07	18	0.10 ± 0.06	4	0.11 ± 0.11	19	0.14 ± 0.07
Cr I	3	-1.17 ± 0.03	6	-0.47 ± 0.05	6	-0.21 ± 0.07	4	-0.20 ± 0.09	10	0.00 ± 0.08
Mn I	2	-1.37 ± 0.13	1	-0.82	–	–	1	-0.58	1	-0.10
Fe I	55	-1.01 ± 0.06	61	-0.43 ± 0.06	73	-0.09 ± 0.06	51	-0.13 ± 0.06	77	0.05 ± 0.06
Fe II	6	-1.08 ± 0.03	3	-0.46 ± 0.02	5	-0.16 ± 0.05	7	-0.25 ± 0.08	7	0.01 ± 0.08
Co I	2	-1.02 ± 0.07	4	-0.39 ± 0.04	5	-0.05 ± 0.07	5	-0.10 ± 0.11	5	-0.03 ± 0.07
Ni I	15	-1.06 ± 0.03	15	-0.42 ± 0.06	25	-0.06 ± 0.06	17	-0.19 ± 0.06	26	0.04 ± 0.07
Y II	–	–	–	–	–	–	–	–	–	–
Zr II	1	-0.52	–	–	1	0.13	–	–	–	–
Ba II	1	-0.41	1	-0.13	1	0.14	1	0.41	1	0.52
La II	1	-0.66	1	-0.40	–	–	1	0.06	2	0.15 ± 0.09
Nd II	2	-0.78 ± 0.09	2	-0.14 ± 0.15	1	0.04	1	0.08	1	0.21
Eu II	1	-0.77	1	-0.12	1	0.15	1	0.08	1	0.34

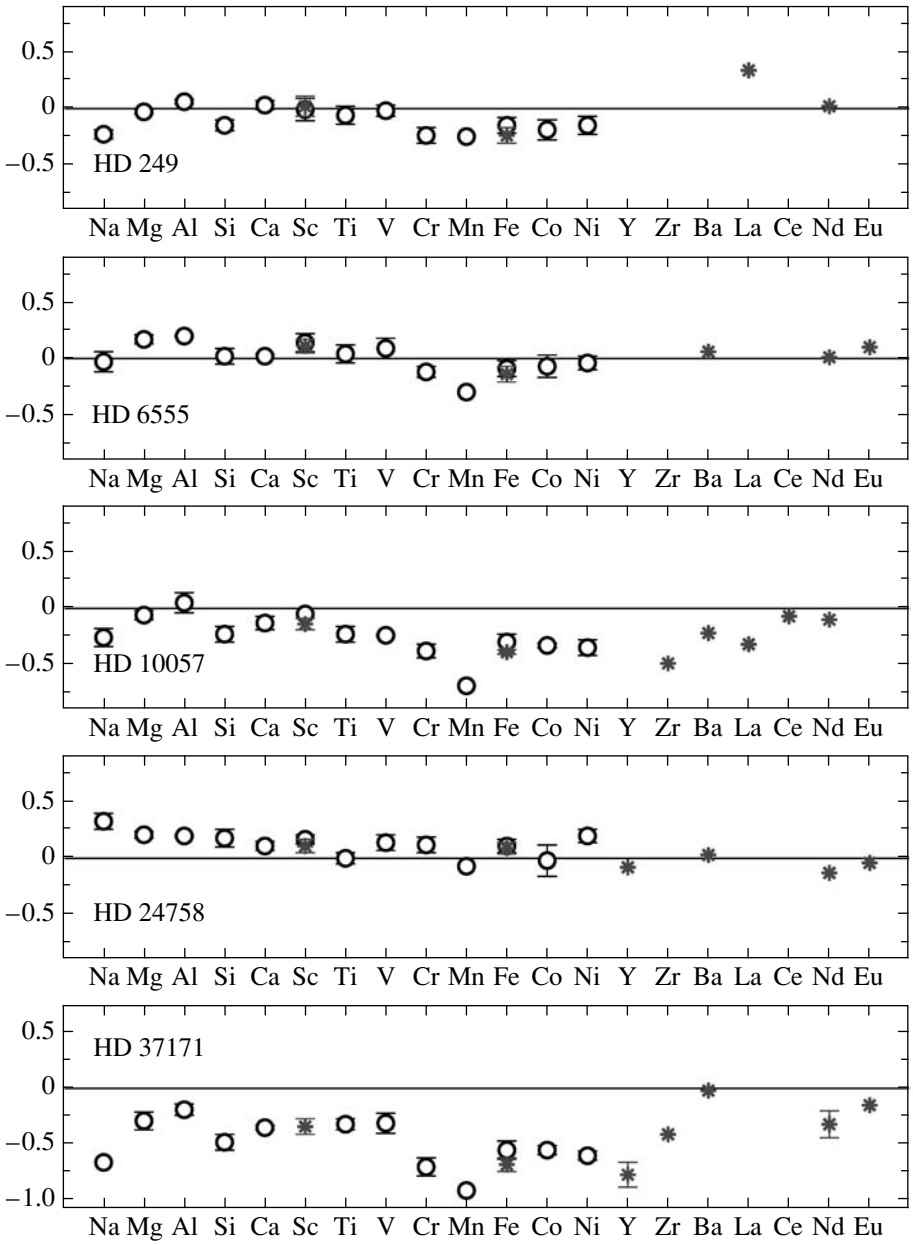

Fig. 1. Relative elemental abundances in the atmospheres of the investigated stars. The circles and asterisks mark the abundances determined from the spectral lines of neutral atoms and ions, respectively.

The sodium abundance was determined from the NaI 6154 Å and 6160 Å lines without any correction for non-LTE processes. According to Korotin and Komarov (1989), Mashonkina et al. (2000), and Lind et al. (2011), this doublet is formed deeper than other sodium lines, and the non-LTE processes do not introduce significant deviations in the abundance determination (<0.1 dex).

Figure 2 presents the abundance trends for some elements with metallicity. The large circles mark our thick-disk red giants with their ordinal numbers from Table 1. The small filled circles indicate the 74 thin-disk red giants from Antipova and Boyarchuk (2001), Boyarchuk et al. (2002), Antipova et al. (2003, 2004, 2005), and Pakhomov et al. (2009) that we studied previously by a unified technique. The filled and open triangles indicate the thin-disk (29 stars) and thick-disk (22 stars) red giants from Alves-Brito et al. (2010), who investiged the Galactic chemical evolution in the solar neighborhood. The solid and dashed lines indicate the thin- and thick-disk dwarfs from Bensby et al. (2005) averaged with a metallicity interval of 0.2 dex, while the shaded region denote a dispersion of 1σ.

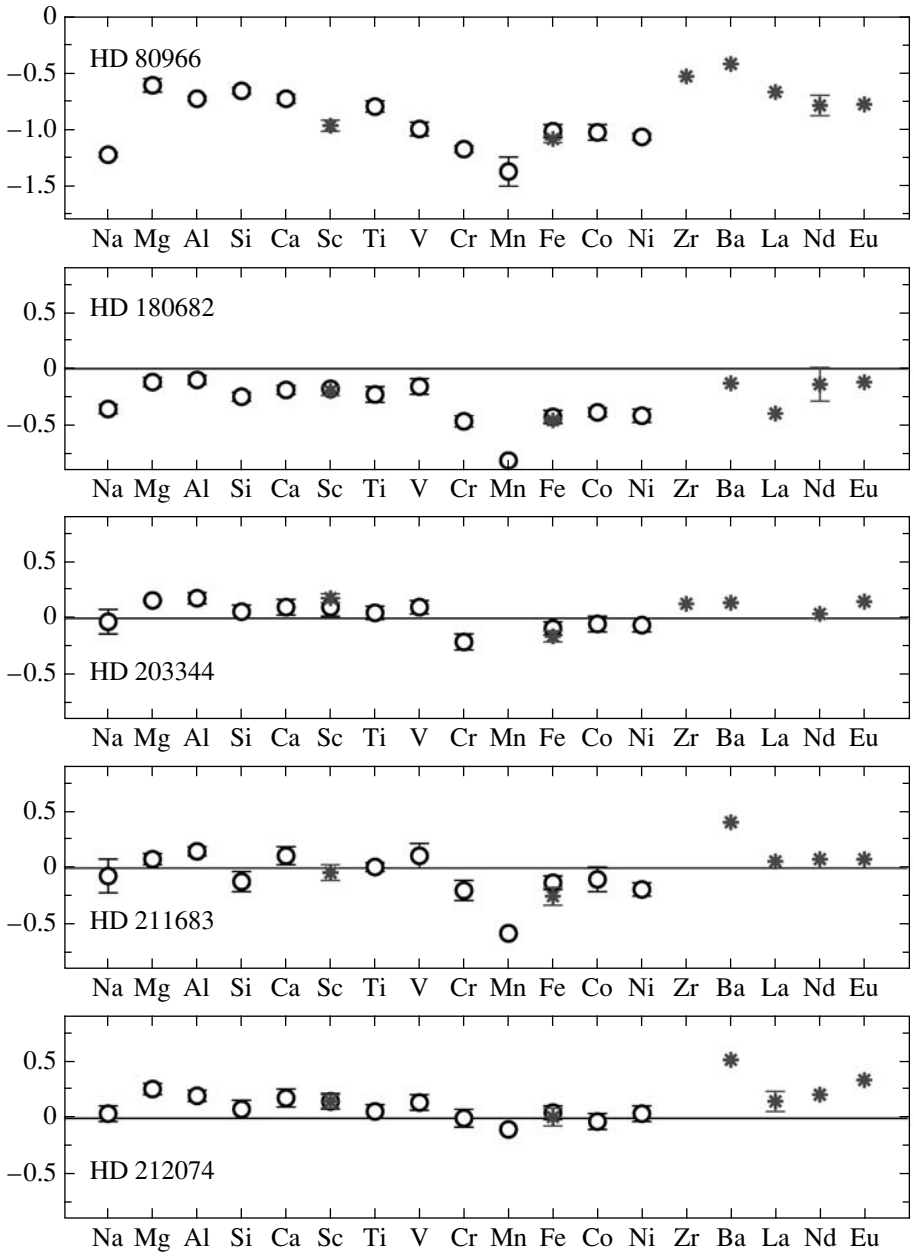

Fig. 1. Contd.

DISCUSSION

Figure 2 demonstrates a compact arrangement of stars for all elements, except sodium, which reflects the evolution of elemental abundances in the Galaxy. The separation of the trends constructed for the thin and thick disks is characteristics of all elements, except sodium. Both dwarfs and giants of each of the disks are located in the same regions, i.e., the abundances of these elements do not change over the elapsed lifetime of the star.

In the case of sodium, a compact arrangement is observed only for dwarfs. The trends for thin- and thick-disk stars coincide, within the error limits. In contrast, red giants are chaotically scattered and no dependence on metallicity can be distinguished. Such a behavior suggests that the [Na/Fe] abundance is determined not only by the chemical evolution of the Galaxy but also by the evolution of the star itself. The amount of sodium that was synthesized in the stellar core at the main-sequence stage and that was brought by convective flows into the stellar atmosphere is added to the initial abundance. The thick-disk red giants in Fig. 2, within the error limits, are located in the region of dwarfs and exhibit no detectable sodium overabundances. However, this is

Table 5. Changes of the elemental abundances in the atmospheres of HD 37171 ($T_{\rm eff} = 4000$ K $\log g = 1.25$ $V_t = 1.35$ km s^{-1}) and HD 212074 ($T_{\rm eff} = 4700$ K $\log g = 2.55$ $V_t = 1.30$ km s^{-1}) when changing the model parameters by $\Delta T_{\rm eff} = +100$ K, $\Delta \log g = +0.10$, $\Delta V_t = +0.10$ km s^{-1} and the total change in abundance Δ

Element	N	Δ[El/H]$_{\rm HD37171}$				N	Δ[El/H]$_{\rm HD212074}$			
		$\Delta T_{\rm eff}$	$\Delta \log g$	ΔV_t	Δ		$\Delta T_{\rm eff}$	$\Delta \log g$	ΔV_t	Δ
NA1	1	0.10	0.00	−0.02	0.10	2	0.10	0.00	−0.02	0.10
MG1	2	−0.02	0.02	−0.01	0.03	2	0.03	0.00	−0.03	0.04
AL1	2	0.08	0.00	−0.03	0.09	2	0.08	0.00	−0.02	0.08
SI1	5	−0.10	0.04	−0.01	0.11	11	−0.04	0.03	−0.01	0.05
CA1	2	0.11	0.00	−0.03	0.11	3	0.08	−0.01	−0.02	0.08
SC2	5	−0.03	0.04	−0.04	0.06	7	−0.02	0.04	−0.03	0.05
TI1	16	0.14	0.01	−0.04	0.15	25	0.14	0.00	−0.03	0.14
V1	3	0.14	0.01	−0.03	0.14	19	0.17	0.01	−0.05	0.18
CR1	7	0.11	0.01	−0.04	0.12	10	0.10	0.00	−0.03	0.10
MN1	1	0.03	0.02	−0.01	0.04	1	0.06	0.01	−0.01	0.06
FE1	34	−0.02	0.03	−0.04	0.05	77	0.04	0.01	−0.04	0.06
FE2	2	−0.21	0.08	−0.03	0.23	7	−0.11	0.06	−0.03	0.13
CO1	4	−0.01	0.03	−0.05	0.06	7	0.06	0.02	−0.05	0.08
NI1	5	−0.06	0.03	−0.04	0.08	26	0.01	0.02	−0.04	0.05
Y2	2	−0.03	0.05	−0.01	0.06					
ZR2	1	−0.03	0.05	0.00	0.06	2	0.20	0.01	−0.01	0.20
BA2	1	0.00	0.00	−0.13	0.13	1	0.02	0.02	−0.10	0.10
ND2	2	0.04	0.04	−0.03	0.06	1	0.03	0.04	−0.02	0.05
EU2	1	0.00	0.05	−0.02	0.05	1	−0.02	0.03	−0.05	0.06

most likely the selection effect, because some of the thick-disk red giants from Alves-Brito et al. (2010) and Pakhomov (2012) have significant [Na/Fe] overabundances.

HD 80966 with the lowest metallicity exhibits the lowest (and atypical of the remaining stars) abundance [Na/Fe] = −0.21 dex with an error of 0.02 dex calculated as the mean of the abundances from the 6154 and 6160 Å lines. Analysis of the possible errors by taking into account the uncertainty in the iron abundance and model parameters leads to a total error of about 0.12 dex. If we explain the low abundance by the error in determining the temperature, then it turns out that we underestimate the temperature approximately by 200 K. Such a change will lead to a significant discrepancy between the elemental abundances determined from lines with different lower-level excitation potentials, while the position of the star on other plots in Fig. 2 will rise dramatically. The discrepancy will also affect the [Fe I/H] and [Fe II/H] abundances, which can be corrected by varying the surface gravity $\log g$. However, the value of $\log g$ determined here is in good agreement with $\log g$ derived from the parallax (1.80 ± 0.15 and 1.86 ± 0.23, respectively).

Nevertheless, the thick-disk giants from our database, on average, exhibit a lower [Na/Fe] abundance than the thin-disk ones: 0.03 ± 0.10 and 0.17 ± 0.15, respectively. Jacobson et al. (2011), who investigated the chemical composition of red giants from two thick-disk open star clusters, NGC 2204 and NGC 2243, also pointed out that at a metallicity [Fe/H] from −0.4 to −0.2 and $\log g$ from 1.5 to 2.9, the mean [Na/Fe] abundance is close to zero: 0.02 ± 0.04.

An increase in the atmospheric [Na/Fe] abundance of red giants is better demonstrated by Fig. 3, which shows the dependence on surface gravity $\log g$. Both these quantities are determined directly from observations. In the figure, the thin-disk stars (filled circles) show a rise as the surface gravity decreases from $\log g \approx 3$–3.5. The surface gravity is related to other fundamental stellar parameters by the relation $\log g = -10.607 + \log M/M_\odot + 4 \log T_{\rm eff} - \log L$, where $M/M_\odot$ is the stellar mass in solar masses and $\log L$ is the stellar luminosity. At a constant stellar mass, the decrease in $\log g$ can be associated with a decrease in the effective temperature and an increase in the stellar luminosity. Such a behavior is typical of a star as it evolves along the red giant branch, and the appearance of sodium overabundances and the increase in sodium abundance due to the rise of sodium-enriched matter through convective flows (Weiss and Charbonnel 2004) are associated precisely with this evolutionary stage.

At this stage of stellar evolution, an enrichment of

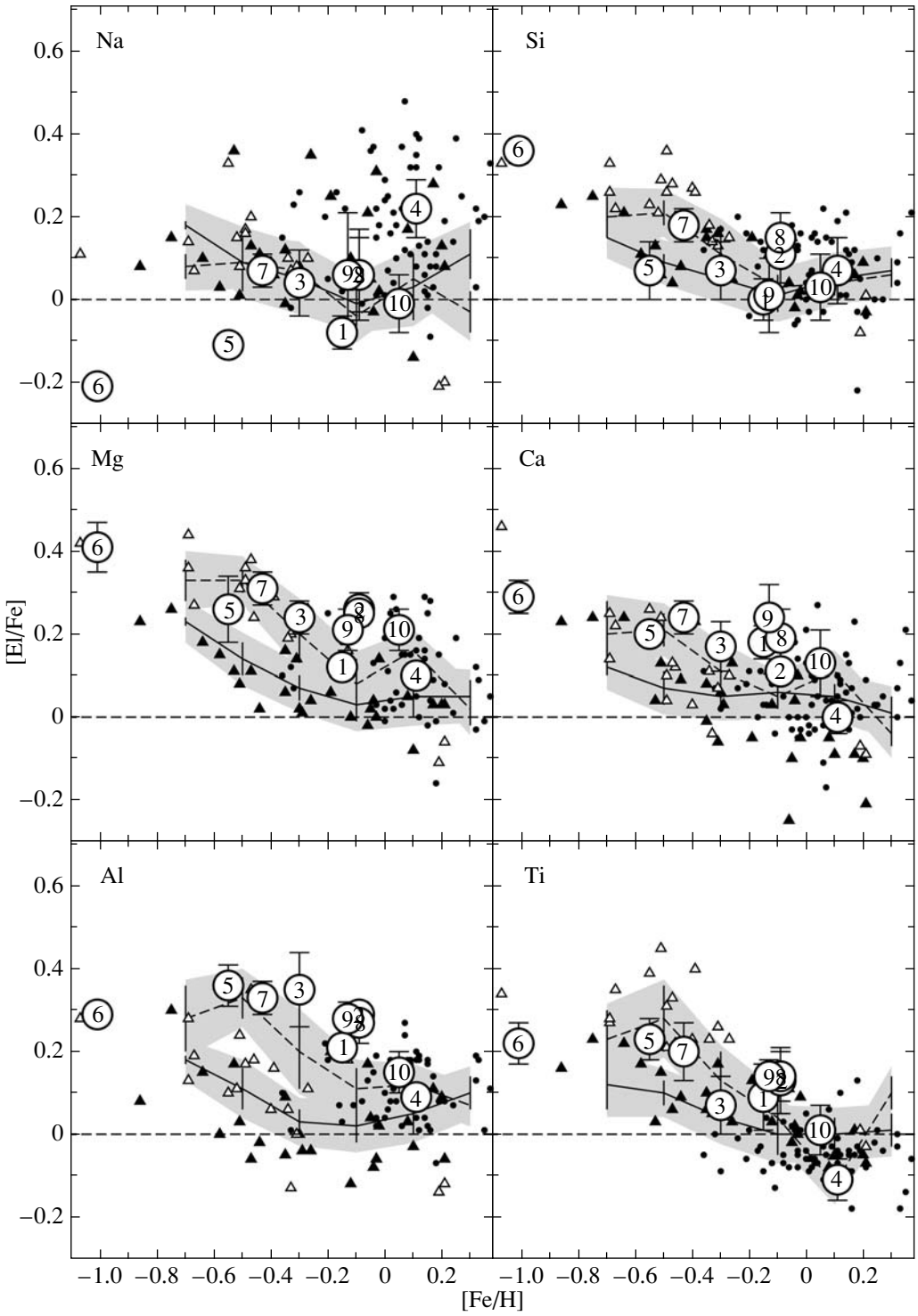

Fig. 2. [Na, Mg, Al, Si, Ca, Ti/Fe] abundance trends with metallicity in the atmospheres of the investigated red giants in comparison with the data for other stars. The small filled circles indicate the thin-disk red giants that we studied previously by a unified technique. The filled and open triangles indicate the thin- and thick disk red giants from Alves-Brito et al. (2010). The solid and dashed lines indicate the thin- and thick-disk dwarfs from Bensby et al. (2005) averaged with a metallicity interval of 0.2 dex; the shaded region denotes a dispersion of 1σ.

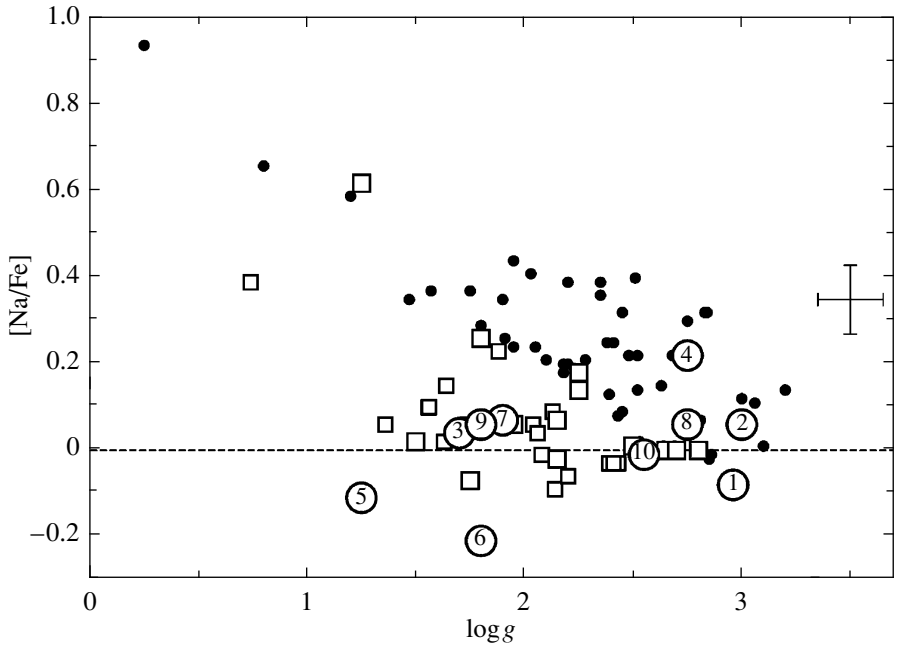

Fig. 3. [Na/Fe] abundance versus surface gravity log g in the atmospheres of the previously investigated thin-disk (filled circles) and thick-disk (open squares) red giants and our red giants (large open circles). The bar of typical errors is indicated on the right.

matter by sodium is possible only in the regions of nuclear reactions at the main-sequence phase. The hydrogen burning reaction in the neon–sodium cycle is the main source of sodium (Cavallo et al. 1996, 1998). In the interiors of low-mass (1–3 $M_\odot$) stars, this cycle is not closed and turns into the chain of reactions ^{20}Ne(p, γ)^{21}Na(β^+)^{21}Ne(p, γ)^{22}Na(β^+)^{22}Ne(p, γ) ^{23}Na.

The first quantitative estimate of these reactions for supergiants is given in Denisenkov and Ivanov (1987): depending on the temperature, from 1/3 to 2/3 of the ^{20}Ne nuclei pass into ^{23}Na. At the same time, the sodium abundance in the atmospheres of F–K supergiants increases by a factor of 5 (0.7 dex), in agreement with the observational data and Fig. 3. Various conditions for the nuclear reactions of the neon–sodium cycle were also considered by Wallerstein et al. (1997) and Takeda and Takada-Hidai (1994).

The thick-disk red giants are marked in Fig. 3 by the large circles (from this paper, the ordinal numbers correspond to Table 1) and squares (previously investigated ones). It can be seen from the figure that they are located systematically below the thin-disk red giants, while for the region $\log g < 2$ the separation between these two groups close in the number of stars exceeds the [Na/Fe] abundance errors. Thus, the difference in [Na/Fe] abundance in the atmospheres of thin- and thick-disk red giants is significant. Among the stars whose parameters were entered into the database, there are several pairs of thin- and thick-disk stars with similar parameters ($T_{\rm eff}$, log g, [Fe/H]) (see Pakhomov 2012). Such stars also have similar masses and ages but differ only by the [Na/Fe] abundance and membership in different kinematic groups of stars in the Galaxy. Such a difference is not observed for the thin- and thick-disk dwarfs (see Fig. 2). Consequently, the initial sodium abundance must be also the same for those stars that have presently become red giants, while the nature of the difference is in the production of sodium in the NeNa cycle. A neon underabundance may exist in thick-disk objects. This is hard to check, because the neon lines are difficult to observe. However, the main ^{20}Ne isotope is an α-process element, and its behavior with metallicity must follow the trends of other α-elements, i.e., an increase in abundance with decreasing metallicity (Alibés et al. 2001). In this case, we should have seen higher overabundances of sodium formed from neon in thick-disk giants, but the reverse is true. The ^{22}Ne underabundance is a possible cause. Indeed, Wallerstein et al. (1997) point out a significant reprocessing of ^{22}Ne into ^{23}Na, while the initial ^{22}Ne/^{23}Na abundance ratio in dwarfs is about 4.1. In any case, the difference between the atmospheric [Na/Fe] abundances of thin- and thick-disk red giants requires an explanation and invoking theoretical calculations.

CONCLUSIONS

Thus, based on spectroscopic observations, we determined the stellar atmosphere parameters for ten

thick-disk red giants. We confirmed the difference in atmospheric [Na/Fe] abundance between thin- and thick-disk giants. Its nature may be related to the neon isotope abundance difference and this hypothesis requires verification.

ACKNOWLEDGMENTS

This work was supported by the Program for Support of Leading Scientific Schools (project NSh-3602.2012.2), the "Nonstationary Phenomena in Objects of the Universe" Program of the Presidium of the Russian Academy of Sciences, and the Federal Agency for Science and Innovations (2012-1.5-12-000-1011-014 "Influence of the Formation of Exoplanets on the Observed Properties of Outer Stellar Layers").

REFERENCES

1. A. Alibés, J. Labay, and R. Canal, Astron. Astrophys. **370**, 1103 (2001).
2. C. Allen and A. Santillan, Rev. Mexic. Astron. Astrofis. **22**, 255 (1991).
3. A. Alves-Bbrito, J. Meléndez, M. Asplund, et al., Astron. Astrophys. **513**, A35 (2010).
4. L. I. Antipova and A. A. Boyarchuk, Astron. Rep. **45**, 700 (2001).
5. L. I. Antipova, A. A. Boyarchuk, Yu. V. Pakhomov, et al., Astron. Rep. **47**, 648 (2003).
6. L. I. Antipova, A. A. Boyarchuk, Yu. V. Pakhomov, et al., Astron. Rep. **48**, 597 (2004).
7. L. I. Antipova, A. A. Boyarchuk, Yu. V. Pakhomov, and M. V. Yushkin, Astron. Rep. **49**, 535 (2005).
8. T. Bensby, S. Feltzing, I. Lundström, et al., Astron. Astrophys. **433**, 185 (2005).
9. M. S. Bessell, F. Castelli, and B. Plez, Astron. Astrophys. **333**, 231 (1998).
10. A. A. Boyarchuk and M. E. Boyarchuk, Izv. KrAO **63**, 68 (1981).
11. A. A. Boyarchuk and L. S. Lyubimkov, Izv. KrAO **64**, 1 (1981).
12. A. A. Boyarchuk and L. S. Lyubimkov, Izv. KrAO **66**, 130 (1983).
13. A. A. Boyarchuk, L. I. Antipova, M. E. Boyarchuk, and I. S. Savanov, Astron. Rep. **45**, 301 (2001).
14. A. A. Boyarchuk, L. I. Antipova, Yu. V. Pakhomov, et al., Astron. Rep. **46**, 819 (2002).
15. A. A. Boyarchuk, L. I. Antipova, and Yu. V. Pakhomov, Astron. Rep. **52**, 630 (2008).
16. F. Castelli and R. L. Kurucz, in *New Grids of ATLAS9 Model Atmospheres, IAU Symp. 210,* Ed. by N. E. Piskunov, W. W. Weiss, and D. F. Gray (2003), p. 20.
17. R. M. Cavallo, A. V. Sweigart, and R. A. Bell, Astrophys. J. **464**, L79 (1996).
18. R. M. Cavallo, A. V. Sweigart, and R. A. Bell, Astrophys. J. **492**, 575 (1998).
19. G. Cayrel and R. Cayrel, Astrophys. J. **137**, 431 (1963).
20. G. Cayrel de Strobel, J. Chauve-Godard, G. Hernandez, et al., Astron. Astrophys. **7**, 408 (1970).
21. B. Chen, C. Stoughton, J. A. Smith, et al., Astrophys. J. **553**, 184 (2001).
22. P. A. Denisenkov, Sov. Astron. **14**, 435 (1988).
23. P. A. Denisenkov and V. V. Ivanov, Sov. Astron. Lett. **13**, 214 (1987).
24. B. Famaey, A. Jorissen, X. Luri, et al., Astron. Astrophys. **430**, 165 (2005).
25. G. Gilmore and N. Reid, Mon. Not. R. Astron. Soc. **202**, 1025 (1983).
26. L. Girardi, A. Bressan, G. Bertelli, et al., Astron. Astrophys. Suppl. Ser. **141**, 371 (2000).
27. T. F. Greene, Astron. J. Suppl. **73**, 15 (1968).
28. J. L. Greenstein and P. C. Keenan, Astrophys. J. **127**, 172 (1958)
29. H. L. Helfer, G. Wallerstein, J. L. Greenstein, Astrophys. J. **129**, 700 (1959).
30. H. L. Helfer and G. Wallerstein, Astrophys. J. Suppl. Ser. **9**, 81 (1964).
31. H. L. Helfer and G. Wallerstein, Astrophys. J. Suppl. **16**, 1 (1968).
32. H. R. Jacobson, E. D. Friel, C. A. Pilachowski, Astron. J. **141**, 58 (2011).
33. S. A. Korotin and N. S. Komarov, Sov. Astron. **33**, 449 (1989).
34. R. Kurucz, *ATLAS9 Stellar Atmosphere Programs and 2 km/s Grid,* Kurucz CD-ROM No. 13 (Smithsonian Astrophys. Obser., Cambridge, MA, 1993), Vol. 13.
35. F. van Leeuwen, Astron. Astrophys. **474**, 653 (2007).
36. K. Lind, M. Asplund, P. S. Barklem, et al., Astron. Astrophys. **528**, A103 (2011).
37. L. I. Mashonkina, V. V. Shimanskii, and N. A. Sakhibullin, Astron. Rep. **44**, 790 (2000).
38. E. Maurice, J. Andersen, A. Ardeberg, et al., Astron. Astrophys. Suppl. Ser. **67**, 423 (1987).
39. T. V. Mishenina, C. Soubiran, V. V. Kovtyukh, et al., Astron. Astrophys. **418**, 551 (2004).
40. Yu. V. Pakhomov, Astron. Lett. **38**, 101 (2012).
41. Yu. V. Pakhomov, L. I. Antipova, A. A. Boyarchuk, et al., Astron. Rep. **47**, 660 (2009a).
42. Yu. V. Pakhomov, L. I. Antipova, A. A. Boyarchuk, et al., Astron. Rep. **49**, 685 (2009b).
43. Yu. V. Pakhomov, L. I. Antipova, and A. A. Boyarchuk, Astron. Rep. **55**, 256 (2011).
44. A. C. Robin, M. Haywood, M. Creze, et al., Astron. Astrophys. **305**, 125 (1996).
45. J. D. Schopp, Astron. J. **59**, 192 (1954).
46. R. Smiljanic, Mon. Not. R. Astron. Soc. **422**, 1562 (2012).
47. Y. Takeda and M. Takada-Hidai, Publ. Astron. Soc. Jpn. **46**, 395 (1994).
48. G. Wallerstein, I. Iben, P. Parker, et al., Rev. Mod. Phys. **69**, 995 (1997).
49. A. Weiss and C. Charbonnel, Mem. Soc. Astron. Ital. **75**, 347 (2004).

Translated by V. Astakhov